Performance Evaluation of Rician Fading Channels using QPSK, DQPSK and OQPSK Modulation Schemes in Simulink Environment

P.Sunil Kumar[1], Dr.M.G.Sumithra[2], Ms.M.Sarumathi

[1](Department of ECE Bannari Amman Institute of Technology, India)
[2](Department of ECE, Bannari Amman Institute of Technology, India)
[3](Department of ECE, Bannari Amman Institute of Technology, India)

ABSTRACT : *Fading is a term used to describe the rapid fluctuations of the amplitudes, phases, or multipath delays of a radio signal over a short interval of time or travel distance, so that large-scale path loss effects may be completely ignored. When there is a dominant stationary signal component present, such as a line-of-sight propagation path, the small-scale fading envelope distribution is Ricean. Digital modulation techniques such as QPSK, DQPSK and OQPSK are dealt in this paper to analyze the characteristics of Rician fading channels in terms of the Bit Error Rate and the implementation is done in the Simulink environment. The paper begins with an overall review on the different type of models for estimating the propagation loss, followed by the different channel models in wireless standards and finally the analysis of Ricean fading characteristics for the different type of modulation schemes is discussed.*

Keywords: DQPSK, Fading, OQPSK, Rician, QPSK

I.   INTRODUCTION

The underpinning principle for electromagnetic wave propagation is Maxwell's equations. Examples of solutions of Maxwell's equations over very large terrain profiles can be found in [1, 2]. However, due to the complex environment of wireless channels that produce reflected, diffracted, or scattered copies of the transmitted signal, analysis based on Maxwell's equations is extremely complex and also impractical since it has to be based on a lot of assumptions. This section describes a number of models, mainly empirical models, for estimating the propagation loss.

I.1 Free-Space Loss:

In free space, the propagation loss from the transmit antenna to the receive antenna can be derived by the Friis power transmission equation [3]

$$P_r(s) = P_t G_t G_r (\frac{\lambda}{4\pi s})^2 \qquad (1)$$

where s is the distance between the transmit and receiver antennas, G*r* and G*t* are the gains of the receive and transmit antennas, respectively, P_t ,P_r are the transmitted and received power, and λ is the wavelength of the carrier frequency. Thus, the power decays as s^{-2}.

I.2 PLANE EARTH LOSS MODEL:

The plane earth model as an s^{-4} power law, is a popular empirical law in wireless communications [4, V, 6, 7]. Measurement in macro cells typically gets a path loss exponent that is close to 4.This model assumes a main path accompanied by a ground-reflected path. The distance difference of the two paths s_2 and s_1 is given by the following expression

$$s_2 - s_1 \approx \frac{2h_t h_r}{s} \qquad (2)$$

Where s is the ground distance between the transmit and receive antennas, and ht, hr are the heights of the transmit and receive antennas respectively.

I.3 OKUMARA-HATA MODEL:

The Okumara-Hata model is a good, but more complex propagation model that is based on extensive empirical measurements taken in urban environments [8], and was further approximated by Hata [9]. The model includes parameters such as frequency, frequency range, heights of the transmitter and receiver, and building

density. The model is the most popular model for macro cell loss prediction. The model for urban areas was standardized in ITU-R Rec.P.V29.

Based on the clutter and terrain conditions, the model varies. The loss is given mathematically as follows [9,7]

$$L = (69.55 + 26.16 \log_{10} f_c - 13.82 \log_{10} h_t) + 44.9 - 6.55 \log_{10} h_t) \log_{10} s - C (dB) \tag{3}$$

where s (in km) is the distance between the transmitter and receiver h_t (in m) is the BS height, h_r (in m) is the MS height, f_c (in MHz) is the carrier frequency, and C is expressed mathematically by the following expression

$$C = 2 \log_{10}^2 (\frac{f_c}{28}) + 5.4 \tag{4}$$

I.4 COST-231-HATA MODEL:

The COST-231 model is an extension of the Okmara-Hata model to 2 GHz. It is also an empirical model, and is suitable for micro cells and small macro cells. This model is suitable when f_c is within 1.V GHz-2 GHz, h_t is within 30-200m, hr is within 1-10 m, and d is within 1-20 km. It is used by the ITU-R IMT-2000 standards for the outdoor case. The COST-231 model is given by [10, 4] as follows

$$L_{urban} = (46.3 + 33.9 \log_{10} f_c - 13.82 \log_{10} h_t) + 44.9 - 6.55 \log_{10} h_t) \log_{10}(d) - C + C_M (dB)$$
(V)

where C is the correction factor for mobile antenna height in urban areas, as defined for small to medium-sized cities, and for larger cities at frequencies fc>300 MHz, C_M is 0 dB for medium-sized cities and suburbs, and 3 dB for metropolitan areas. Although both the Okumara-Hata and COST-231-Hata models are specified to have a BS antenna height above 30m, they can be used when ht is less than 30m, as long as the surrounding buildings are well below this height. They are not suitable for microcells like urban canyons.

I.V COST-231- WALFISCH-IKEGAMI MODEL:

Although the plane earth model has a path loss exponent close to measurement, the two-path model is inapplicable since the MS typically operates without the MS typically operates without a LOS path or a ground reflection. In fact, in most cases, diffraction is a major propagation mechanism. A number of physical models based on diffraction analysis, such as the Ikegami model [11], the flat-edge model, and the Walfisch- Bertoni model[12], are discussed in [7]. Theoretical analysis from these physical models can also yield a path-loss exponent close to 4, but provides more insight into the propagation mechanism. The COST-231-Walfisch-Ikegami (COST-WI) model combines the Walfisch-Bertoni model and the Ikegami model plus some empirical correction factors to improve the agreement with the measurements in the urban environment [10, 13].

I.6 INDOOR PROPAGATION MODELS:

Indoor propagation models must be considered for PCS. Indoor radio propagation is dominated by the same mechanisms as the outdoor, but the conditions are more variable inside a building. House and office buildings have different internal and external structures. The wide variety in partitions as well as their physical and electrical characteristics makes it very difficult to find a general model to a specific indoor environment. ITU-R Rec.P.1238 [14] gives a total path loss model for propagation within buildings

$$L = 20 \log_{10} f_c + 10\eta \log_{10} r + L_f (n_f) - 28 (dB) \tag{6}$$

where η is the path loss component, $L_f (n_f)$ is the floor penetration loss, which varies with the number of penetrated floors n_f. Corresponding parameters are given in [14]. COSTM-231 also has some models for indoor multi-wall propagation and propagation into buildings [10].

I.7 EXTENDED SALEH-VALENZUELA MODEL:

The well-known Saleh-Valenzuela indoor channel model [1V] was based on measurements utilizing low power ultra-short pulses (of width 10 ns and centre frequency 1.V GHz) in a medium-size, two-story office building [1V]. In this model, multipath components arrive in groups (clusters), or in rays within a cluster. Cluster arrivals are Poisson-distributed with rate ∂. Within each cluster, ray arrivals are also Poisson distributed. This model requires four parameters, namely the cluster arrival rate ∂, the ray arrival rate within a cluster $\lambda (\lambda > \partial)$, the cluster decay factor Γ and the ray decay factor γ. It is thus observed that clustering also takes place in the angular domain [16].

I.8 RAY-TRACING:

Ray-tracing or geometrical optics and the uniform theory of diffraction (UTD) techniques are usually used to approximate the accurate solution based on Maxwell's equations. The error of geometrical optics approximation is very small when the receiver is many wavelengths away from the scatter, or when all the

scatters are smooth and large compared to a wavelength. The ray representation of radio propagation is especially useful at microwave and millimeter wave bands. This method is appropriate for characterizing radio wave propagation in cities, since the wavelength is much smaller compared to the dimensions of the buildings.

II.   CHANNEL MODELS IN WIRELESS STANDARDS

The European COST-2V9 directional antenna model was developed as an empirical model for simulation of systems with multiple antennas at either the BS or the MS. The model takes into account small-scale as well as large-scale effects, and covers the macro, micro and pico cellular scenarios. The European project COST-273 extends the COST-2V9 model to the double-directional case.

The COST-273 model is suitable as a space-time model. The 3GPP channel model [17], which is based on COST-273, is widely used for modeling the outdoor macro and microcell wireless environments. It is suitable for WiMAX, and can be used for other systems such as IEEE 802.11n and 802.20., with minor modifications to the parameters. The 3GPP channel model uses too many parameters to build a fully empirical channel model. 3GPP2 provides simpler semi-empirical channel models. It defines pedestrian A and pedestrian B models for low-mobility pedestrian mobile users (at 3km/hr), and a vehicular A and vehicular B models for higher mobility vehicular mobile users (at 30 km/hr). These models define the multipath profiles according to the number of multipath taps, and the power and delay of each multipath component. Each multipath component is modelled as an independent Rayleigh fading, and the correlation in the time domain is due to the Doppler effect of the specified speed.

The Erceg model [18] was obtained based on extensive measurement at 1.9 GHz in 9V macro cells across the USA. It has three modes: Erceg A for hilly terrain with moderate to heavy tree density, Erceg B for hilly terrain with light tree density or flat density with moderate to heavy tree density, and Erceg C for flat terrain with light tree density. The Erceg model is valid for the frequency range 1900-3V00 MHz, BS height 10-80m, MS height 2-10 m, and distance 100m-8km. These models correspond to the six SUI channel models: SUI-1 to SUI-6, with terrain type C corresponding to SUI-1 and SUI-2 terrain type B to SUI-3 and SUI-4, and terrain type A to SUI-V and SUI-6. The Erceg model is applicable for fixed wireless deployment with MS installed under the eave or on the rooftop, and has been adopted in IEEE 802.16 for fixed broadband applications [19].

The IEEE 802.11 TGn models [21] are a set of models, which are an improved and standardized version of the extended Saleh-Valenzuela model, with overlapping delay clusters. The models are for indoor MIMO wireless LANs at both 2 and V GHz and for bandwidths of upto 100 MHz. Six canonical channels are modelled, namely, flat fading, residential, small-office, typical office, large office, and large open spaces. For each canonical channel, the number of clusters, the values of the DoD (direction-of-departure) and DoA (direction-of-arrival) and the cluster angular spreads are fixed, and the tap-delay profiles are represented in the delay domain. The ITU channel models, unlike the 3GPP channel model, do not model any correlation between the fading waveforms across the transmit and receive antennas. These models were developed for single-input single-output channels. They are also widely used for link-level and system-level performance simulation of 1x EV-DO and HSDPA. In case of correlation of multiple antennas, correlation matrices can be multiplied with the channel matrix H at both the transmit and receive ends. ITU has specified two multipath profiles (A and B) for vehicular, pedestrian, and indoor channels, respectively. Channel A is suitable for urban macro-cellular environments, while channel B is suitable for modeling rural macro cells and microcells with cell radius less than V00 m.

III.   CHANNEL FADING

There are usually three types of channel fading for mobile communications: shadowing (slow fading), multipath Rayleigh fading, and frequency-selective fading. Reflection, diffraction, and scattering are the three major mechanisms that influence the signal propagation.

III.1 RAYLEIGH FADING:

For wireless communications, the envelope of the carrier signal is Rayleigh distributed; and such a type of fading is thus called Rayleigh fading. This can be caused by multipath with or without the Doppler effect. In the multipath case, when the dominant signal becomes weaker, such as in the non-LOS case, the received signal is the sum of many components that are reflected from the surroundings. These independent scattered signal components have different amplitudes and phases (time delays); then, I and Q components of the received signal can be assumed to be independent zero-mean Gaussian processes. This is derived from the central limit theorem, which states that the sum of a sufficient number of random variables approaches very closely to a normal distribution. When the MS moves, the frequency shift of each reflected signal component that arises from the

Doppler effect also has an influence on the fading. Successive drops in amplitudes occur at distances of $\frac{\lambda}{2}$ that is, every time period of $\frac{\lambda}{2v}$ where λ is the wavelength of the carrier frequency and v is the speed of the MS. Since the I and Q components of the received signal are i.i.d. zero mean Gaussian random variables, the phase at any time instant is uniformly distributed and is mathematically given as

$$\rho_\phi(\phi) = \frac{1}{\pi}, -\pi \le \phi \le \pi \tag{7}$$

Rayleigh fading occurs very rapidly, and hence it occurs very rapidly, and hence it is known as fast fading. It can cause as much as 30 to V0 dB rapid power fluctuations at a scale that is comparable to one wavelength, and is thus referred as small-scale fading. The multipath model is commonly modelled as a two-ray model for illustrating Rayleigh fading. The impulse response is given by [6] and is expressed as follows

$$h(t) = \alpha_1 e^{j\theta_1(t)}\delta(t) + \alpha_2 e^{j\theta_2(t)}\delta(t-\tau) \tag{8}$$

where α_1 and α_2 are independent random variables with a Rayleigh pdf, θ_1 and θ_2 are two independent random variables with uniform pdf over [0 to 2π] and τ is the time delay. The received signal is composed of multipath components. The different delays of these components lead to a multipath delay spread. If the time differences of these components are significant compared to one symbol period, intersymbol interference (ISI) occurs. The multipath delay spread has a spectrum with null magnitudes at frequency intervals of $1/\tau$, where τ is the time delay. Thus, this type of fading is called frequency-selective fading. When the delay spread is much less than a symbol period, the channel is said to exhibit flat fading.

III.2 RICEAN FADING:

When a strong stationary path such as a line of sight path is introduced into the Rayleigh fading environment, the fading becomes Rice-distributed fading. Ricean fading is suitable for characterizing satellite communications or in some urban environments. Ricean fading is also a small-scale fading. In this case, the probability of deep fade is much smaller than that in the Rayleigh Fading case. Based on the central limit theorem, the joint pdf of amplitude r and phase ϕ may be represented as derived in [V] as follows

$$\rho_{r,\phi}(r,\phi) = \frac{r}{2\pi\sigma^2} e^{-\frac{r^2+A^2-2rA\cos\phi}{2\sigma^2}} \tag{9}$$

where A is the amplitude of the dominant component and σ is the same as that for Rayleigh fading,. This joint pdf is not separable, and the pdf of r or ϕ can be obtained by integrating over the other quantity. The pdf of the amplitude is a Rice distribution [21] and is mathematically expressed as follows

$$\rho_r(r) = \frac{r}{\sigma^2} e^{-\frac{r+A^2}{2\sigma^2}} I_0(\frac{rA}{\sigma^2}), 0 \le r < \infty \tag{10}$$

where $Z_0(x)$ is the modified Bessel function of the first kind and zero order, and is defined as follows

$$Z_0(x) = \frac{1}{2\pi}\int_0^{2\pi} e^{-x\cos\theta}d\theta \tag{11}$$

The mean square value of r is given by

$$\rho_r = 2\sigma^2 + A^2 \tag{12}$$

The Rice factor Kr is defined as the ratio of the dominant component to the power in all the other components and it is given by the equation $K_r = \frac{A^2}{2\sigma^2}$. The Rice distribution approximates the Rayleigh distribution with mean value A as Kr<<1, and reduces to it at Kr=0. It approximates the Gaussian distribution with mean value A as Kr>>1, and reduces to the Gaussian as $K_r \to \infty$. The factor Kr typically shows an exponential decrease with range, and varies from 20 near the BS to zero at a large distance[22]. The dominant component changes the phase distribution from the uniformly random distribution of Rayleigh fading to clustering around the phase of the dominant component. The stronger the dominant component, the closer the resulting phase to the phase of the dominant component. This is similar to a delta function. Flat Ricean fading channel is suitable for characterizing a real satellite link.

IV. PHASE SHIFT KEYING MODULATION SCHEMES

In phase shift keying techniques (PSK), change in phase of the carrier signal is used for the representation of 0 and 1 bits. The transmission of bit 0 is represented by the presence of the carrier for a specific interval of time, while the transmission of bit 1 is represented by the presence of a carrier signal with a phase difference of π radians for the same interval of time. PSK using a cosine carrier wave with amplitude Lc, and frequency fc can be mathematically represented as follows

$$i(t) = L_c \cos(2\pi f_c t + \pi), binary1$$

$$i(t) = L_c \cos(2\pi f_c t), binary0$$

This technique is also known as binary PSK (BPSK) or two-level PSK since a single phase difference is used for representing 0 and 1 bits. Just as multiple frequency levels are used in FSK, multiple phase deviations can be used in PSK. This enables encoding of multiple bits by each phase representation. Quadrature PSK (QPSK), for example, uses four different phases each separated by π/2 radians. This would enable transmission of two bits per phase shift. The mathematical representation of QPSK is given below.

$$i(t) = L_c \cos(2\pi f_c t + \frac{\pi}{4}), binary10$$

$$i(t) = L_c \cos(2\pi f_c t + \frac{3\pi}{4}), binary11$$

$$i(t) = L_c \cos(2\pi f_c t + \frac{5\pi}{4}), binary01$$

$$i(t) = L_c \cos(2\pi f_c t + \frac{7\pi}{4}), binary00$$

π/4 shifted QPSK is a type of mechanism where the maximum phase deviation is limited to $\pm 13V$ degrees. The main utility of π/4 shifted QPSK is that it can be received in a non-coherent manner, that is, the receiver need not lock to the phase of the transmitted signal, which simplifies the design of the receiver to a great extent. It provides the similar bandwidth efficiency of QPSK and also the amplitude will not suffer from more fluctuations. π/4 shifted QPSK is used in the North American digital cellular TDMA standard, IS-136, and also in the Japanese digital cellular(JDC) standard. Differential PSK is a variation of the basic PSK mechanism. Here, binary 1 is represented by the presence of a carrier signal whose phase has been changed relative to the phase of the carrier used for representing the previous bit. A binary 0 is represented by the presence of a carrier wave whose phase is the same as that of the carrier used for transmitting the previous bit. DPSK comes with an advantage. Since phase differences occur continuously for long runs of 1s , this can be used for self-clocking. If there are only two possible phase differences, used for representing bit 0 and bit 1, then the modulation technique is called differential binary PSK (DBPSK).If four phase differences are used, for representing the bit sequences 00,01,10,11, then the scheme is called differential quadrature PSK (DQPSK). If a greater number of phase differences are used, say, 8 or 16, is used then the corresponding systems are called 8-DPSK and 16-DPSK, respectively/4-DQPSK is another modulation technique, which is a variant of the DQPSK technique. In π/4-DQPSK, an additional phase shift of π/4 radians is inserted in each symbol. In standard DQPSK, a long run of zeros at the data input would result in a signal with no phase shifts at all, which makes synchronization at the receiver very difficult. If π/4-DQPSK is used in such a situation, the phase shift of π/4 ensures that there is a phase transition for every symbol, which would enable the receiver to perform timing recovery and synchronization. Another variant of PSK is π/4 shifted PSK (π/4psk). A pair of bits is represented by varying the phase of the carrier signal relative to the phase of the carrier signal used for representing the preceding pair of bits. Offset QPSK which is also sometimes called as staggered quadrature phase-shift keying (SQPSK) is a variant of phase-keying modulation technique where four different values of the phase to transmit is being utilized. Consideration of the four values of the phase, that is, two bits at a time to construct a QPSK symbol can allow the phase of a signal to jump by as much as 180 degrees at a time. When the signal is passed through a low-pass filter, then these phase-shifts results in large amplitude fluctuations, which is an undesirable quality in communication systems. The best way to overcome this problem is to offset the timing of the odd and even bits by one or half bit per period, then the corresponding in phase and quadrature phase components will never change at the same time. This type of mechanism results in a much lower amplitude fluctuations than non-offset QPSK and is mainly deployed in practice.

V. PERFORMANCE ANALYSIS USING SIMULINK

The environment is created as shown in the figures 1, 2, 3 respectively using Simulink tool.

V.1 RANDOM INTEGER GENERATOR: The random integer generator generates random uniformly distributed integers in the range [0, M-1], where M is the M-ary number.

V.2. INTEGER TO BIT CONVERTER: In the integer to bit convertor unit, a vector of integer-valued or fixed valued type is mapped to a vector of bits. The number of bits per integer parameter value present in the integer to bit convertor block defines how many bits are mapped for each integer-valued input. For fixed-point inputs, the stored integer value is used. This block is single-rated and so the input can be either a scalar or a frame-based column vector. For sample-based scalar input, the output is a 1-D signal with 'Number if bits per integer' elements. For frame-based column vector input, the output is a column vector with length equal to 'Number of bits per integer' times larger than the input signal length.

V.3 DIFFERENTIAL ENCODER: Differential encoder differentially encodes the input data. The differential encoder object encodes the binary input signal within a channel. The output is the logical difference between the current input element and the previous output element.

V.4 CONVOLUTIONAL INTERLEAVER: This block permutes the symbols in the input signal. Internally, it uses a set of shift registers. The delay value of the kth shift register is (k-1) times the register length step parameter. The number of shift registers is the value of the rows of shift registers parameter.

V.5 DQPSK MODULATOR: The DQPSK modulator baseband modulates the input signal using the differential quaternary phase shift keying method.

V.6 DQPSK DEMODULATOR: The DQPSK demodulator baseband demodulates the input signal using the differential quaternary phase shift keying method

V.7 OQPSK MODULATOR: The OQPSK modulator baseband modulates the input signal using the offset quaternary phase shift keying method

V.8 OQPSK DEMODULATOR: The OQPSK Demodulator baseband demodulates the input signal using the offset quaternary phase shift keying method.

V.9 QPSK MODULATOR: The QPSK modulator baseband modulates the input signal using the quaternary phase shift keying method.

V.10 QPSK DEMODULATOR: The QPSK demodulator baseband demodulates the input signal using the quaternary phase shift keying method.

V.11 BUFFER: The buffer converts scalar samples to a frame output at a lower sample rate. The conversion of a frame to a larger size or smaller size with optional overlap is possible. It is then passed to the multipath Rician fading

V.12 CONVOLUTIONAL DEINTERLEAVER: The Convolutional deinterleaver block recovers a signal that was interleaved using the Convolutional interleaver block.

V.13 DIFFERENTIAL DECODER: The differential decoder block decodes the binary input signal.

V.14 BIT TO INTEGER CONVERTER: The bit to integer converter maps a vector of bits to a corresponding vector of integer values. The number of bits per integer parameter defines how many bits are mapped for each output.

V.15 ERROR RATE CALCULATION: The error rate calculation is done by computing the error rate of the received data by comparing it to a delayed version of the transmitted data.

V.16 SIGNAL TRAJECTORY SCOPE: The discrete-time signal trajectory scope is used to display a modulated signal constellation in its signal space by plotting the in phase component versus the quadrature component.

V.17 SCATTER PLOT SCOPE: The discrete-time scatter plot scope is used to display a modulated signal constellation in its signal space by plotting the in phase component versus the quadrature component.

V.18 EYE DIAGRAM SCOPE: The discrete-time eye diagram scope displays multiple traces of a modulated signal to reveal the modulation characteristics such as pulse shaping, as well as channel distortions of the signal.

V.19 SNR ESTIMATION: The SNR estimation block gives the estimated SNR in decibels.

V.20 DISPLAY: This unit gives the total number of bits transmitted, the number of errors and finally displays the Bit Error Rate.
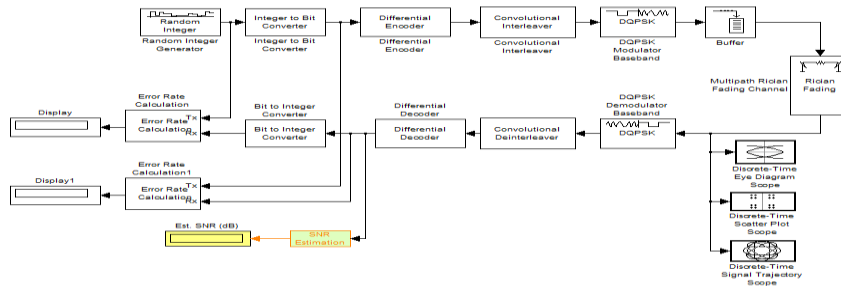
Fig. 1. Simulink diagram for the performance analysis of Rician fading channels in DQPSK modulation
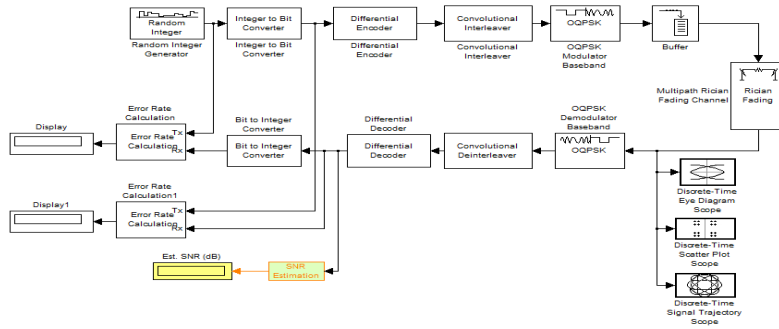

Fig. 2. Simulink diagram for the performance analysis of Rician fading channels in OQPSK modulation
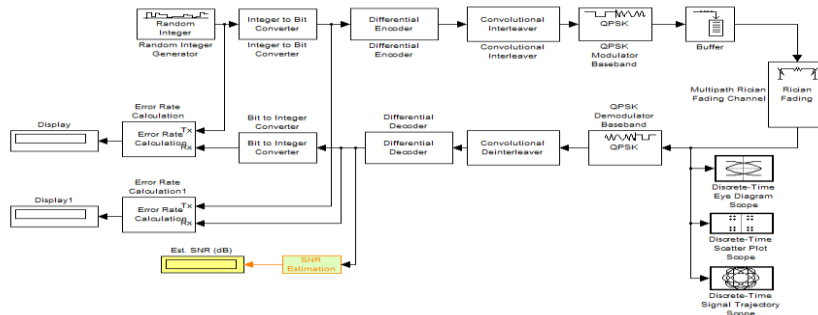

Fig. 3. Simulink diagram for the performance analysis of Rician fading channels in QPSK modulation
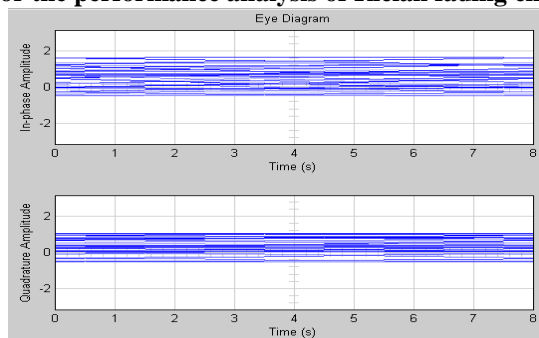

Fig. 4. Eye diagram for performance analysis of Rician fading channel in DQPSK
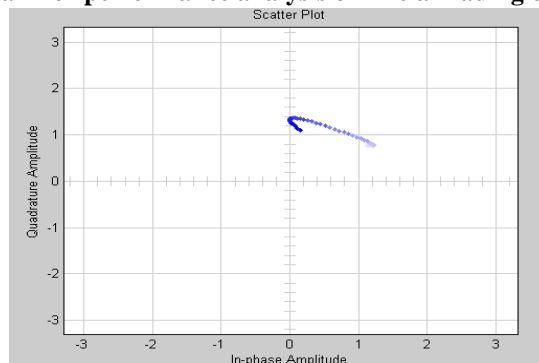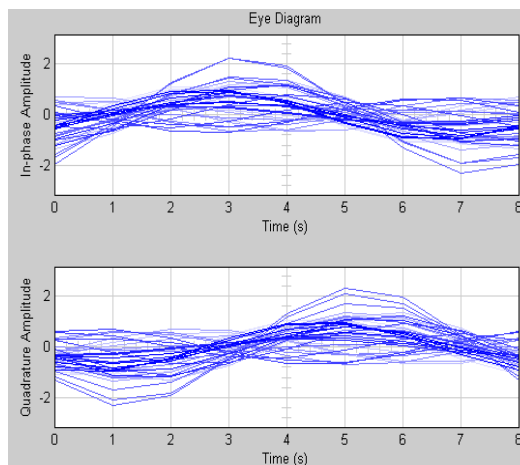

Fig. V. Scatter plot for performance analysis of Rician fading channel in DQPSK

Table 1: BER for Rician fading channels in DQPSK

SNR(dB)	BER
3	0.004410
V	0.003627
7	0.002167
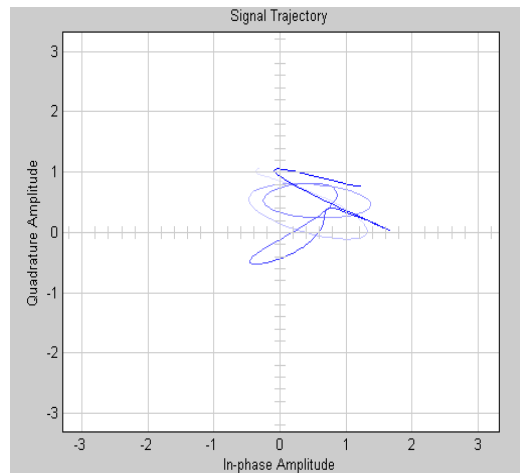
Fig. 6. Signal trajectory for performance analysis of Rician Fading channels in DQPSK

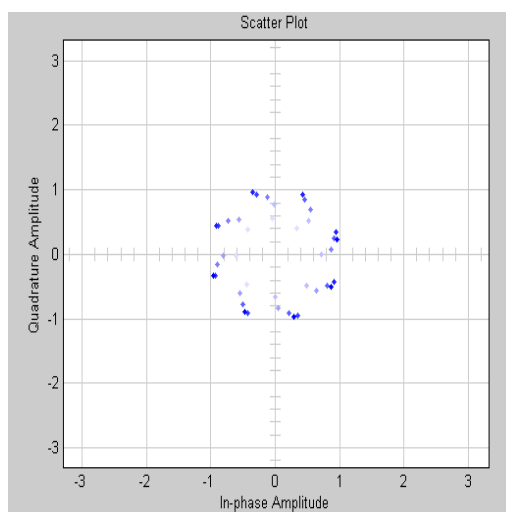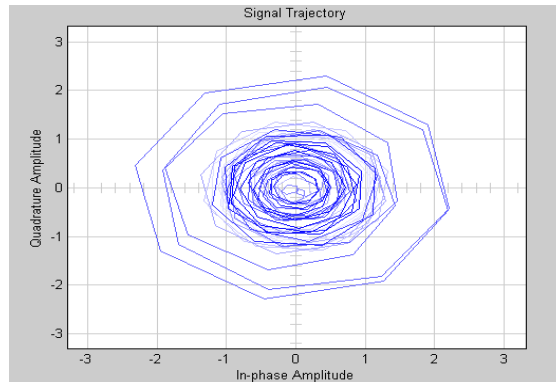**Fig. 7. Eye diagram for performance analysis of Rician fading channels in OQPSK**

Fig. 8. Scatter plot for performance analysis in Rician fading channels in OQPSK

Table2:BERfor Rician fading channels in OQPSK

SNR(dB)	BER
3	0.3V1V
V	0.3260
7	0.2948

Fig. 9. Signal Trajectory for performance analysis of Rician fading channels in OQPSK
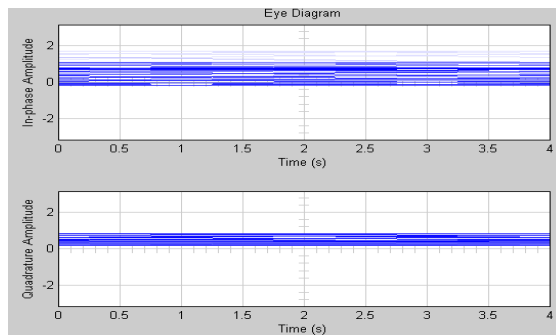

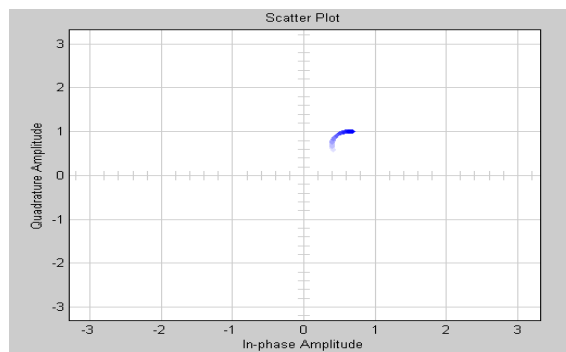**Fig. 10. Eye diagram for performance analysis of Rician fading channels in QPSK**

Fig. 11. Scatter plot for performance analysis of Rician fading channels in QPSK

Table 3: BER for Rician fading channels in QPSK

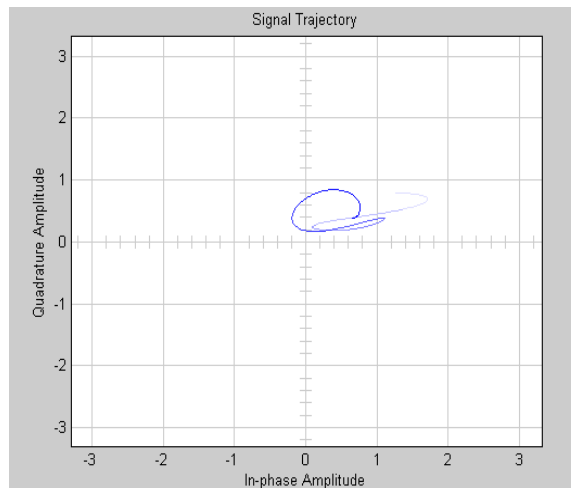| SNR(dB)	BER
3	0.3046
V	0.2881
7	0.0677V

Fig. 12. Signal trajectory for the performance analysis of Rician fading channels in QPSK

VI.   CONCLUSIONS

A Comprehensive Literature Survey on the different types of models for estimating the propagation loss, followed by the different channel models in wireless standards is reviewed in this paper. The analysis of Rician fading channels in modulation schemes like DQPSK, OQPSK and QPSK is discussed and the results are provided. It is evident from table 1, table 2, and table 3 that when the Signal-to-Noise Ratio increases, the Bit error rate naturally decreases. The Eye diagram, signal trajectory diagram and the scatter plot diagram have also been provided for the scenario. Out of the three modulation schemes DQPSK produces a very low bit error rate when Rician channel is characterized. Future works may include finding the bit error rate by evaluating the performance of Rician fading channels in other different types of modulation schemes.

REFERENCES

[1].   C.A.Tunc, A.Altintas and V.B.Erturk, Estimation of existent propagation models over large inhomogeneous terrain profiles using fast integral equation solution. *IEEE Trans.Anten. Propagation*.,V3:9(200V), 3080-3083.

[2].   A.Yagbasan, C.A.Tunc, V.B.Erturk, A.Altinas and R.Mitra, Use of characteristic basis function method for scattering from terrain profiles. *Turk. J.Electr.Eng*.,16:1 (2008), 33-39.

[3].   D.M.Pozar, *Microwave Engineering*, 3 rd edn (New York: Wiley, 200V).

[4].   A.Goldsmith, *Wireless Communication* (Cambridge, UK:Cambridge University Press,200V)

[5].   A.F.Molisch, *Wireless Communications* (Chichester: Wiley-IEEE,200V).

[6].   T.S.Rappaport, *Wireless Communication: Principles and Practise,* 2nd edn (Upper Saddle River, NJ:Prentice Hall PTR, 2002)

[7].   S.R.Saunders and A.Aragon-Zavala, *Antennas and Propagation for Wireless Communication Systems,* 2nd edn (Chichester, England:Wiley,2007)

[8].   Y.Okumara, E.Ohmori, T.Kawano and K.Fukuda, Field strength and its variability in VHF and UHF land mohile radio service. Rev. *Electr.Commun. Lab*(1968), 82V-873

[9].   M.Hata, Empirical formula for propagation loss in land mobile radio services. *IEEE Trans. Veh.Tech.*, 29:3(1980), 317-32V.

[10].   COST 231, Digital Mobile Radio Toward Future Generation Systems, *Final Report, European Commisision*, Brussels, 1999.

[11].   F.Ikegami, T.Takeuchi and S.Yoshida, Theoretical prediction of mean field strength for urban mobile radio. *IEEE Trans. Anten.Propagat*., 39:3 (1991), 299-302.

[12].   J.Walfisch and H.L.Bertoni, A theretical model of UHF propagation in urban environments. *IEEE Trans. Anten. Propagat.,* 36:12(1988), 1788-1796.

[13].   D.Har. A.W.Watson and A.G.Chadney, Comments on diffraction loss of rooftop-to-street in COST 231 Walfish-Ikegami model. *IEEE Trans. Veh. Tech.*,48:V(1999), 14V1-14V2.

[14].   ITU-R, Propagation Data and Prediction Models for the planning of Indoor Radio-communication Systems and Radio Local Area Networks in the Frequency Range 900 MHz to 1000 GHz, *ITU-R Rec.P.1238*,Geneva, 1997.

[15].   A.A.M.Saleh and R.A.Valenzuela, A statistical model for indoor multipath propagation. *IEEE J.Sel. Areas Commun*., V:2(1987), 1281C-137.

[16].   Q.H.Spencer, B.D.Jeffs, M.A.Jensen and L.Swindlehurst, Modeling the statistical time and angle of arrival characteristics of an indoor multiple channel. *IEEE J.Sel.Areas.Commun*., 18:3(2000), 347-360.

[17].   3GPP, Technical Specification Group Radio Access Network. Spatial Channel Model for Multiple Input Multiple Output(MIMO) Simulations*, 3GPP TR 2V.996 V6.1.0, technical report*, Sep 2003.

[18].   V.Erceg, L.J.Greenstein, S.Y.Tjandra, S.R.Parkoff, A.Gupta, B.Kulic, A.A.Julius and R.Bianchi, An empirically based pathloss model fro wireless channels in suburban environments. *IEEE J.Sel.Areas.Commun*., 17:7(1999), 120V-1211.

[19].   V.Erceg, et al, Channel Models for Fixed Wireless Applications, *Rev. 4.0, IEEE802.16.3c-01/29r4, IEEE*, Jul 2001.

[20].   S.O.Rice, Statistical properties of a sine wave plus random noise. *Bell Syst. Tech.J.*,27:1 (1948), 109-1V7.

[21].   A.Paulraj, R.Nabar and D.Gore, *Introduction to Space-Time Wireless Communications* (Cambridge, UK:Cambridge University Press, 2003)